Journal of Atmospheric and Solar–Terrestrial Physics 271 (2025) 106527

Contents lists available at ScienceDirect

Journal of Atmospheric and Solar-Terrestrial Physics

journal homepage: www.elsevier.com/locate/jastp

Research Paper

Analysis of laser beam propagation through atmospheric turbulence and its impact on CCD sensor intensity distribution

Maryam Jafari, Masoud Mollaee *, Khashayar Heshmati Jannat Magham, Mahmoud Rezaee Rokanabadi

Ferdowsi University of Mashhad, Department of Physics, Mashhad, Iran

ARTICLE INFO

Handling Editor: Dora Pancheva

Keywords:
Atmospheric turbulence
CCD sensor
Gaussian beam
Laguerre Gaussian
Laser propagation
Photon detection

ABSTRACT

This study investigates the propagation of laser beams with Gaussian and Laguerre-Gaussian profiles through atmospheric turbulence and their subsequent detection by charge-coupled device (CCD) sensors. Using numerical simulations based on the Kolmogorov turbulence model, we analyze the intensity distribution of laser beams under turbulence strengths ranging from 10^{-16} to 10^{-12} and propagation distances of 500 m to 5 km. The effects of atmospheric turbulence on photon distribution at the CCD sensor's pixels are quantified, revealing beam broadening with Full Width at Half Maximum (FWHM) increasing from 50 μm to 1.5 m under the highest turbulence conditions. Saturation and blooming phenomena are observed, with photon density exceeding 10^6 photons/pixel in high-intensity regions. Our findings reveal that turbulence-induced distortions significantly impact beam intensity profiles, with higher turbulence levels causing up to a 70 % reduction in central intensity. Additionally, the study highlights the sensitivity of higher-order Laguerre-Gaussian modes, which exhibit up to 90 % greater broadening compared to fundamental Gaussian modes. By evaluating the impact of aperture size and f-number on beam focusing, we show that increasing the f-number from 2 to 8 reduces saturation artifacts by 60 % while spreading intensity over a larger area.

1. Introduction

The propagation of laser beams in the earth's atmosphere create several challenges, primarily due to the presence of atmospheric turbulence. There have been many interests in studying random effects in laser beam propagation through atmosphere (Andrews et al., 2001; Salem et al., 2004; Yahel and Last, 1992; Ronchi et al., 1970). This disturbance can cause beam spreading, flickering and beam deflection, which significantly affect the quality and resolution of laser beam detection systems. Understanding the effect of such turbulence on the intensity distribution of laser beams reaching the Charge-Coupled Device (CCD) sensor is very important for the optimization of remote sensing, imaging and communication technologies (Korotkova et al., 2004), (Shaik, 1988).

Numerous studies have investigated laser beam propagation through turbulent media. Andrew et al., in their comprehensive work (Andrews and Phillips, 2005)laid the foundation for understanding the behavior of laser beams in turbulent atmospheres. Their research highlighted the impact of random media on beam quality and provided valuable insights into the underlying mechanisms of beam degradation. Hashemipour et al. (2012) investigated the effects of atmospheric disturbances like attenuation, scattering, turbulence, and thermal blooming on laser beam propagation. They modeled vertical beam propagation and generate the average intensity profile. Their results demonstrated that atmospheric turbulence, thermal blooming (for high-power lasers), and beam diameter significantly affect the peak intensity of the laser beam. Huang et al. (2015) extended beam wander theory to non-Kolmogorov turbulence and derived a general analytical expression. Their work showed that beam wander is influenced by turbulence parameters and the laser beam's initial conditions. By analyzing Gaussian Schell model array beams, they found that beam wander increases with a decreasing inner scale, increasing outer scale, and variations in the generalized exponent parameter. It decreases with greater beam separation, a higher number of beams, and lower coherence. They concluded that adjusting these parameters could mitigate beam wander. Luo et al. (Luo and Han, 2020) applied the Generalized Huygens–Fresnel principle and Rytov approximation to study vortex beam arrays. Their results indicated that vortex beam arrays are less susceptible to turbulence than single vortex beams.

* Corresponding author.
E-mail address: m.mollaee@um.ac.ir (M. Mollaee).

https://doi.org/10.1016/j.jastp.2025.106527
Received 8 October 2024; Received in revised form 2 March 2025; Accepted 26 April 2025
Available online 3 May 2025

They also observed that the mean square beam widths of the beamlets converge over time, with the evolution strongly influenced by turbulence intensity and topological charge. In another work (Ata, 2022) analytical expressions for the wave structure function, coherence length, and angle-of-arrival variance of a Gaussian beam in underwater turbulence were derived using a recent oceanic turbulence model. The authors analyzed the effects of temperature, salinity, dissipation rates, and other factors, and compared the Gaussian beam's performance to plane and spherical waves. The scintillation index of Hermite Gaussian beams in air vehicle communication systems through weak atmospheric turbulence was investigated using the modified Rytov method (Sayan et al., 2020). The study analyzed how the scintillation index changes with beam size, propagation distance, and zenith angles for uplink and downlink paths.

While these contributions have advanced the field, they leave critical gaps in understanding the interaction between beam profiles and turbulence effects when reaching to a CCD sensor—and the resulting implications for sensor performance—remain underexplored. The present study addresses this gap by focusing on the numerical simulation of laser beam propagation with Gaussian and Laguerre-Gaussian profiles through atmospheric turbulence. Using the Kolmogorov spectrum to model turbulence, this work calculates the beam intensity distributions and evaluates their impact on CCD sensor imaging quality. By analyzing how turbulence-induced distortions affect photon detection, the study provides practical insights for optimizing laser-based systems.

This work is distinct in its comprehensive approach to examining both Gaussian and Laguerre-Gaussian beam profiles in turbulent conditions and their subsequent detection by CCD sensors. The methodology integrates numerical simulations with established turbulence models, offering detailed assessments of intensity distributions and photon counts at the pixel level. Such analysis is critical for improving the design of laser systems in applications ranging from free-space optical communication to advanced imaging systems.

2. Theory

According to the Kolmogorov theory, atmospheric turbulence can be considered as a cascade of eddies or swirling fluid elements of different sizes. These eddies are constantly generated and quickly dissipate, contributing to the random variations in the refractive index of the air. The refractive index variations, in turn, introduce phase distortions to light waves passing through the atmosphere.

The effects of atmospheric turbulence on the Gaussian beam can be described using the Rytov approximation, which leads to an expression for the second-order moments of the beam, i.e., the size and position of the beam. Atmospheric disturbance effects cause an additional phase shift along the wavefront and spread the beam beyond its diffraction limits. The Helmholtz equation describes the radiation propagation in turbulence:

$$\nabla^2 \mathrm{U} + \mathrm{n}^2(\mathrm{r})\,\mathrm{k}^2\mathrm{U} = 0 \tag{1}$$

where r is a point in space, $k = 2\pi/\lambda$ and the refractive index of the diffusing medium n(r) is now a function of location. The complete solutions of this equation can be found using the Green's function method in which:

$$\mathrm{U}(\mathrm{r},\mathrm{z}) = -2\mathrm{jk}\iint_{-\infty}^{+\infty} G(s,r,z)U(s,0)d^2s \tag{2}$$

$$\mathrm{G}(\mathrm{s},\mathrm{r},\mathrm{z}) = \frac{1}{4\pi}\exp\left[jkz + \frac{jk}{2z}|s-r|^2\right] \tag{3}$$

Rytov's method can provide closed-form approximations for the solutions of this differential equation. This method assumes that U(r,z) fluctuations are caused by atmospheric turbulence in the form of mixed phase disturbances, so that the solutions of the Helmholtz equation can be written as follows.

$$\mathrm{U}(\mathrm{r},\mathrm{z}) = \mathrm{U}_0(\mathrm{r},\mathrm{z})\,\mathrm{e}^{\varphi(\mathrm{r},\mathrm{z})} = \mathrm{U}_0(\mathrm{r},\mathrm{z})\exp[\varphi_1(\mathrm{r},\mathrm{z}) + \varphi_2(\mathrm{r},\mathrm{z})] \tag{4}$$

Where φ_1 and φ_2 are the first and second order mixed phase perturbations due to turbulence. The additional broadening of the optical beam can be checked by examining the average radiation intensity of the optical beam.

$$\langle I(r,z)\rangle = \langle U(r,z)U^*(r,z)\rangle \tag{5}$$

$$\langle I(r,z)\rangle = \frac{W_0^2}{W^2}\exp\left(\frac{-2r^2}{W^2}\right)\exp\left[2\sigma_r^2(r,z) - t\right] \tag{6}$$

$$\sigma_r^2(r,z) = 0.663\sigma_l^2\Lambda^{5/6}\left[1 - F\left(\frac{-5}{6}.l.\frac{2r^2}{W^2}\right)\right] \tag{7}$$

$$t = 4\pi^2k^2z\int_0^1\int_0^\infty k\Phi_n(\kappa)\left[1 - \exp\left(\frac{-\Lambda z\kappa^2\pounds^2}{k}\right)\right]d\kappa d\pounds \tag{8}$$

$$F(a,c,z) = \sum_{n=0}^{\infty}\frac{a}{c}\frac{z^n}{n!} \tag{9}$$

$$\sigma_l^2 = 1.23C_n^2k^{7/6}z^{11/6} \tag{10}$$

where z is the distance that the wave propagates in a region with constant C_n^2. Using the Kolmogorov spectrum and the following approximation:

$$e^{-t} \approx \frac{1}{(1+t)} \tag{11}$$

$$\frac{r^2}{W^2} - \sigma_r^2(r,z) \approx \frac{r^2}{W^2}(1+t) \tag{12}$$

the average intensity can be approximated:

$$\langle I(r,z)\rangle \approx \frac{W_0^2}{W_e^2}\exp\left(\frac{-2r^2}{W_e^2}\right) \tag{13}$$

$$W_e = W\left(1 + 1.33\sigma_l^2\Lambda^{\frac{5}{6}}\right)^{\frac{1}{2}} \quad \sigma_l^2 < 1 \tag{14}$$

$$W_e = W\left(1 + 1.624\left(\sigma_l^2\right)^{\frac{6}{5}}\Lambda\right)^{\frac{1}{2}} \quad \sigma_l^2 > 1 \tag{15}$$

Now if a collimated gaussian laser beam with beam waist of W_0, and power of P_0 is defined, then the average intensity can be written as follow:

$$\langle I(r,z)\rangle = \frac{W_0^2}{W_e^2}I_0\exp\left(-\frac{2r^2}{W_e^2}\right) \tag{16}$$

$$I_0 = \frac{2P_0}{\pi W_0^2} \tag{17}$$

Thus, as in free space, the average intensity due to turbulence (the above equation) is completely determined by the beam spot size. Depending on the spectrum model, internal scale effects may increase or decrease the spot size, while the external scale always tends to limit its size. However, under conditions of weak fluctuations, the effects of internal and external scale on the beam spot size are usually very small. Therefore, in many practical situations, using the above equation is sufficient to describe the beam spot size due to turbulence.

In the following, the Kolmogorov theory is implemented in our simulation, and the calculated mean intensity distributions of the laser beam propagation for two Gaussian and Laguerre-Gaussian profiles in the atmosphere, as well as their effect on CCD sensor imaging, are presented. A Laguerre-Gaussian beam is a type of laser beam that has a helical phase front that rotates around the beam axis. Assuming cylindrical symmetry, the higher order modes of a collimated beam at the exit aperture (z = 0) of the laser can be described in cylindrical coordinates (r, Θ, z).

$$z = 0 : U_{mn}(r, \theta, 0) = \left(\frac{\sqrt{2}r}{W_0}\right)^m (-i)^m \exp\left(-\frac{r^2}{W_0^2}\right) L_n^{(m)}\left(\frac{2r^2}{W_0^2}\right) \tag{16}$$

Here r is the vector in the transverse plane at angle Θ, W_0 is the radius of the beam, $L_n^{(m)}$ is the associated Lager polynomial, and n and m are the radial and angular mode numbers. The field described by the above equation is called Lager-Gaussian beam. Using the Huygens-Fresnel integral, it can be shown that the Lager-Gaussian beam field obtained at the distance z from the transmitter is as follows:

$$U_{mn}(r, \theta, z) = C_{mn} \frac{W_0}{W_e}\left(\frac{\sqrt{2}r}{W(z)}\right)^m L_n^{(m)}\left(\frac{2r^2}{W(z)^2}\right)\exp[- \mathrm{i}(2\mathrm{n} + \mathrm{m} + 1)\varphi(\mathrm{z})] \times \exp\left(ikz + im\theta - \frac{r^2}{{W_e}^2} - i\frac{kr^2}{2F}\right) m, n = 0, 1, 2, \ldots, \tag{17}$$

where C_{mn} is a trivial phase constant and W and F denote the spot size and radius of curvature of the phase front for a TEM_{00} beam. Intensity deduced from the above equation, adding the initial intensity of laser:

$$I(r, \theta, z) = |U_{mn}(r, \theta, z)|^2 = I_0 \frac{{W_0}^2}{{W_e}^2}\left(\frac{2r^2}{{W_e}^2}\right)^m \left[L_n^{(m)}\left(\frac{2r^2}{{W_e}^2}\right)\right]^2 \exp\left(-\frac{2r^2}{{W_e}^2}\right) \tag{18}$$

3. Results and discussion

Fig. 1 illustrate the radial intensity distribution of laser beams under moderate turbulence conditions $C_n^2 = 10^{-12}$ at propagation distances of L = 500 m, 1000 m, and 2000 m for various beam modes. Each mode exhibits distinct intensity profiles that evolve with distance, revealing key insights into the interplay between mode structure, turbulence, and beam propagation. In the first plot, corresponding to the fundamental mode (m = 0,n = 0), the intensity profile shows a single, symmetric peak centered at r = 0. The peak intensity decreases significantly with increasing L and the beam broadens, redistributing energy over a wider area. This behavior aligns with theoretical expectations of Gaussian beam diffraction and turbulence-induced spreading, highlighting the fundamental mode's suitability for long-distance applications requiring high beam stability and focused energy delivery. The second plot depicts the intensity distribution for the higher-order mode (m = 0,n = 2), characterized by two symmetric peaks. At shorter distances (L = 500 m), the peaks are sharp and distinct, but as the distance increases, the peaks broaden, and their intensity diminishes. At L = 2000 m, the beam structure degrades further, with significant energy dispersion. This indicates that higher-order modes are more vulnerable to turbulence compared to the fundamental mode. Nonetheless, their distinct two-peak structure can be advantageous for specific applications requiring

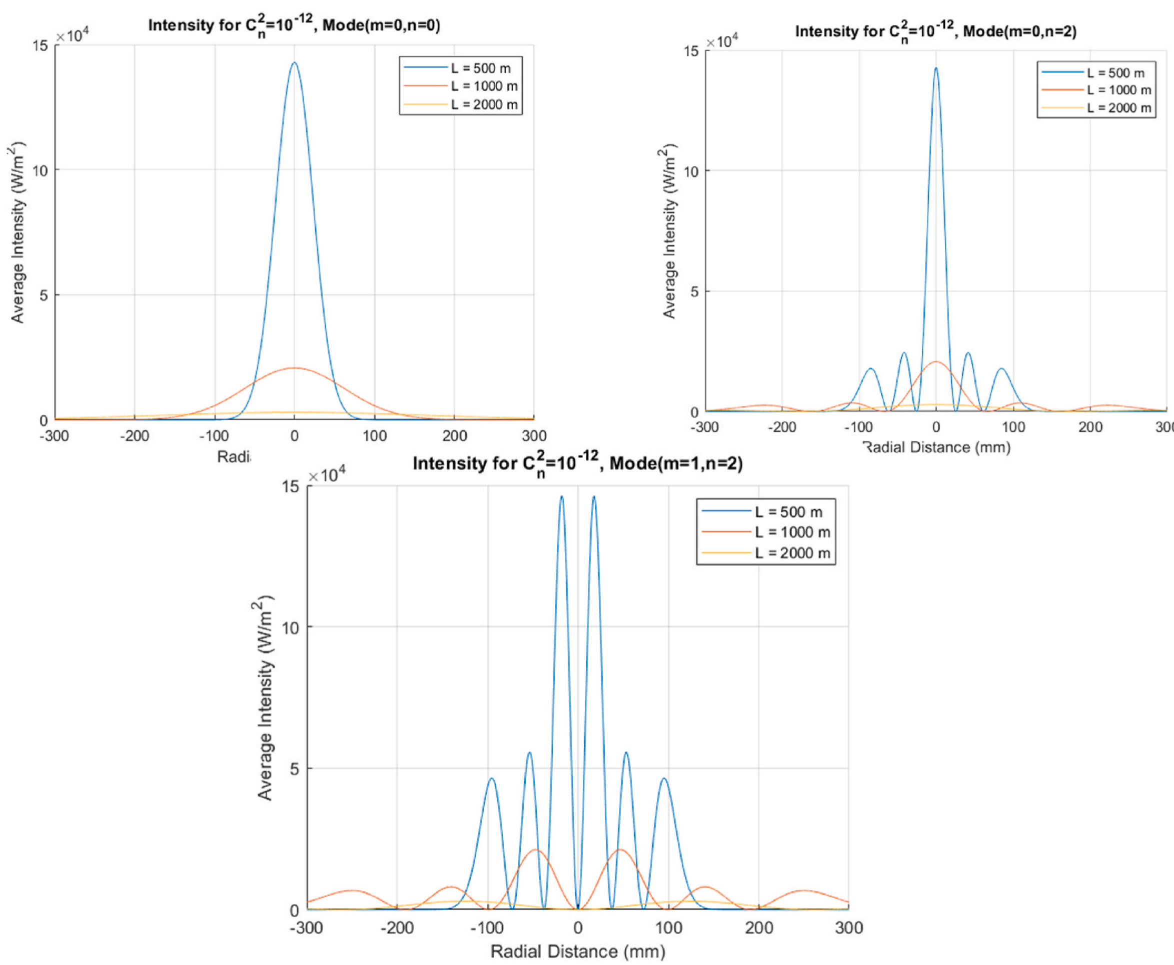

Fig. 1. The Laguerre-Gaussian beam intensity in a turbulent environment with Cn2 = 10–12 for different m, n at distances of 2 km, 1 km and 500 m from the source.

energy deposition at off-axis positions, such as optical manipulation or pattern projection. The third plot, showing the mode (m = 1,n = 2), presents a more complex intensity structure with multiple peaks symmetrically distributed around r = 0. At shorter distances, these peaks are relatively sharp, but as the distance increases, the structure degrades rapidly, with significant broadening and flattening of the intensity distribution. By L = 2000 m, much of the beam's energy is distributed across a wider radial distance, and the intricate pattern becomes less distinct. This highlights the sensitivity of complex modes to turbulence, making them less suitable for long-range applications but potentially useful in near-field applications where structured intensity profiles are desired, such as optical trapping or advanced imaging systems. Comparing all three plots reveals several key trends. As the propagation distance increases, the intensity of all modes diminishes, and the beams broaden due to turbulence-induced phase distortions.

The fundamental mode (m = 0,n = 0) is the most robust, maintaining a compact and focused intensity distribution, while higher-order modes (m,n≠0) degrade faster and exhibit greater beam spreading. This underscores the trade-offs between mode complexity and propagation stability, where simpler modes are ideal for long-range communication and sensing applications, while higher-order modes may be better suited for specialized applications requiring non-uniform energy profiles.

Fig. 2 demonstrates the impact of turbulence strength (C_n^2) on the propagation of a Gaussian beam over a distance of L = 5 km. In Fig. 2a, the radial intensity distributions are shown for various C_n^2 values. At lower turbulence levels ($C_n^2 = 10^{-16}$), the beam retains a sharp, high-intensity peak centered at r = 0, reflecting minimal broadening and energy dispersion. As C_n^2 increases, the central peak diminishes in height and broadens significantly, indicating that stronger turbulence disrupts the wavefront and spreads the beam energy over a wider area. At the highest turbulence level ($C_n^2 = 10^{-12}$, the beam's intensity profile becomes considerably flatter, showing severe degradation in beam quality and a loss of focus. Fig. 2b provides a quantitative analysis of this behavior by plotting the Full Width at Half Maximum (FWHM) of the beam as a function of C_n^2. For very weak turbulence ($C_n^2 = 10^{-15}$), the FWHM remains nearly constant, suggesting negligible beam distortion. However, as C_n^2 increases beyond 10^{-15}, the FWHM grows exponentially, reaching over 1500 m at $C_n^2 = 10^{-12}$. This exponential relationship underscores the significant impact of strong turbulence, where small increases in C_n^2 lead to disproportionately large beam spreading. These results highlight the sensitivity of Gaussian beams to atmospheric turbulence. While the beam maintains high spatial resolution and intensity under weak turbulence, its performance degrades rapidly in stronger turbulence. This has practical implications for applications such as free-space optical communication, remote sensing, and laser targeting, where operating in low-turbulence environments or employing turbulence mitigation techniques, such as adaptive optics, becomes essential. The rapid increase in FWHM with C_n^2 underscores the importance of stabilizing beam propagation in turbulent conditions to maintain spatial resolution and intensity.

The schematic illustrated in Fig. 3 which is a setup for analyzing the propagation of a Gaussian laser beam over a distance of 500 m, followed by truncation through an aperture, focusing with a converging lens, and intensity measurement using a CCD sensor. The beam initially exhibits a Gaussian intensity profile that spreads with propagation, as indicated by the color-coded representation, with higher intensities in red and lower intensities in white. The aperture truncates the beam, limiting its diameter and removing peripheral energy, which shapes the beam but also results in some energy loss. When the broadened beam reaches the lens, the lens introduces a quadratic phase shift to the optical field, focusing the beam onto the observation plane located at the lens's focal length. Under ideal conditions, the lens performs a Fourier transform of the beam's field at the aperture, producing a focused spot. However, due to turbulence-induced broadening, the beam entering the lens has a larger waist, which directly impacts the size and sharpness of the focal spot.

The modulus of the complex wave amplitude of the Gaussian beam after the aperture and lens when observation plane and focal plane is same, can be described as:

$$U_{\text{aperture}}(r) = \sqrt{\frac{2P_0}{\pi W_{\text{LT}}^2\left(1 - e^{-\frac{2a^2}{W_{\text{LT}}^2}}\right)}}\exp\left(-\frac{r^2}{W_{\text{LT}}^2}\right)\exp\left(-i\frac{kr^2}{2f}\right) \quad (19)$$

And for Laguerre gaussian it can be written as:

$$U_{\text{aperture}}(r,\theta) = \sqrt{\frac{2P_0}{\pi W_{\text{LT}}^2\left(1 - e^{-\frac{2a^2}{W_{\text{LT}}^2}}\right)}}\left(\frac{\sqrt{2}r}{W_{\text{LT}}}\right)^{|m|}L_n^{|m|}\left(\frac{2r^2}{W_{\text{LT}}^2}\right)$$
$$\exp\left(-\frac{r^2}{W_{\text{LT}}^2}\right)\exp(-im\theta)\exp\left(-i\frac{kr^2}{2f}\right) \quad (20)$$

Finally, the intensity at the observation plane, where the focal plane is placed can be defined as (Dickson, 1970):

$$I(r_2,f) = \left|\int_0^a U_{\text{aperture}}(r)J_0\left(\frac{2\pi r r_2}{\lambda f}\right)r\,dr\right|^2 \quad (21)$$

The optical field at the aperture was represented as a combination of

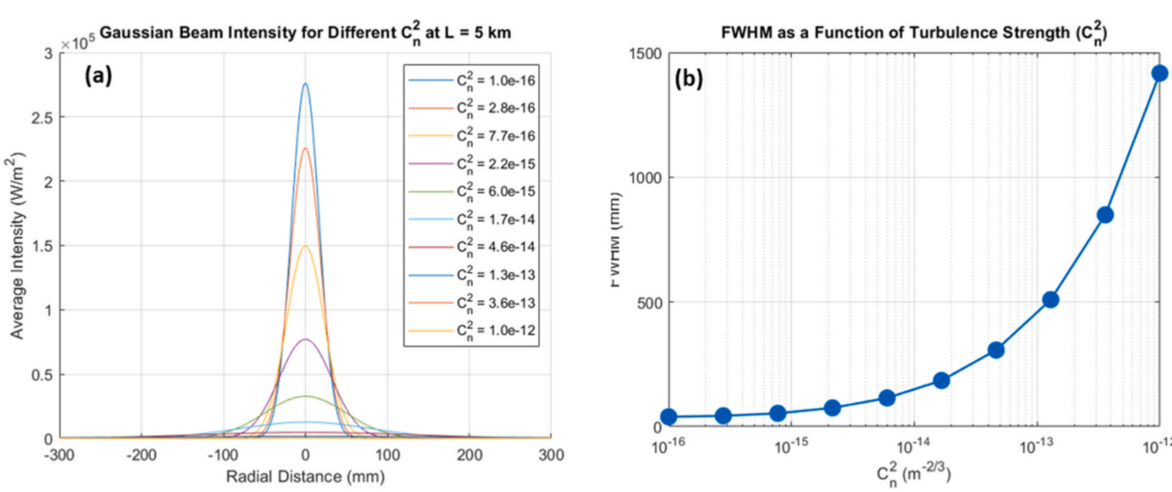

Fig. 2. a) Gaussian beam intensity for different Cn2 at distances of 5 km. b) FWHM as a function of turbulence strength Cn2.

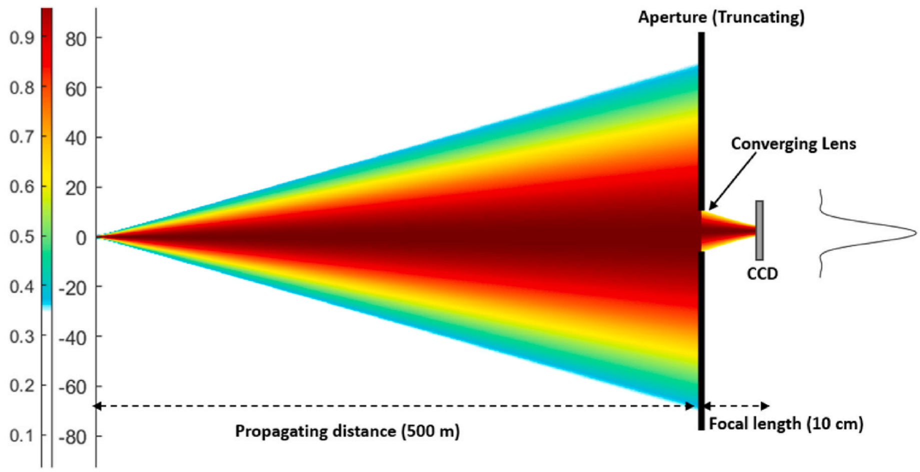

Fig. 3. The scheme of setup.

a Gaussian amplitude distribution, scaled to account for the source power (P_0), and the lens-induced phase factor $\exp\left(-i\frac{kr^2}{2f}\right)$, which is due to quadratic phase of lens. Using the Huygens-Fresnel principle and the Bessel function (J_0), the far-field intensity was obtained numerically by integrating over the aperture radius (a).

To gain a deeper understanding of the image formation process, it is essential to examine the intensity of light reaching the Charge-Coupled Device (CCD) sensor of the camera. The CCD sensor is responsible for converting incident light into electrical signals, which are ultimately used to form the digital image. When light enters the camera through the aperture, it passes through the lens system before reaching the CCD sensor. Each pixel within the CCD measures the intensity of the incoming light, converting it into an electrical charge proportional to the number of interacting photons. The calculation of the photon count per pixel involves several factors, including the intensity of the incident light, exposure time, camera sensitivity, and sensor efficiency. To estimate the number of photons per pixel, the incident light intensity is

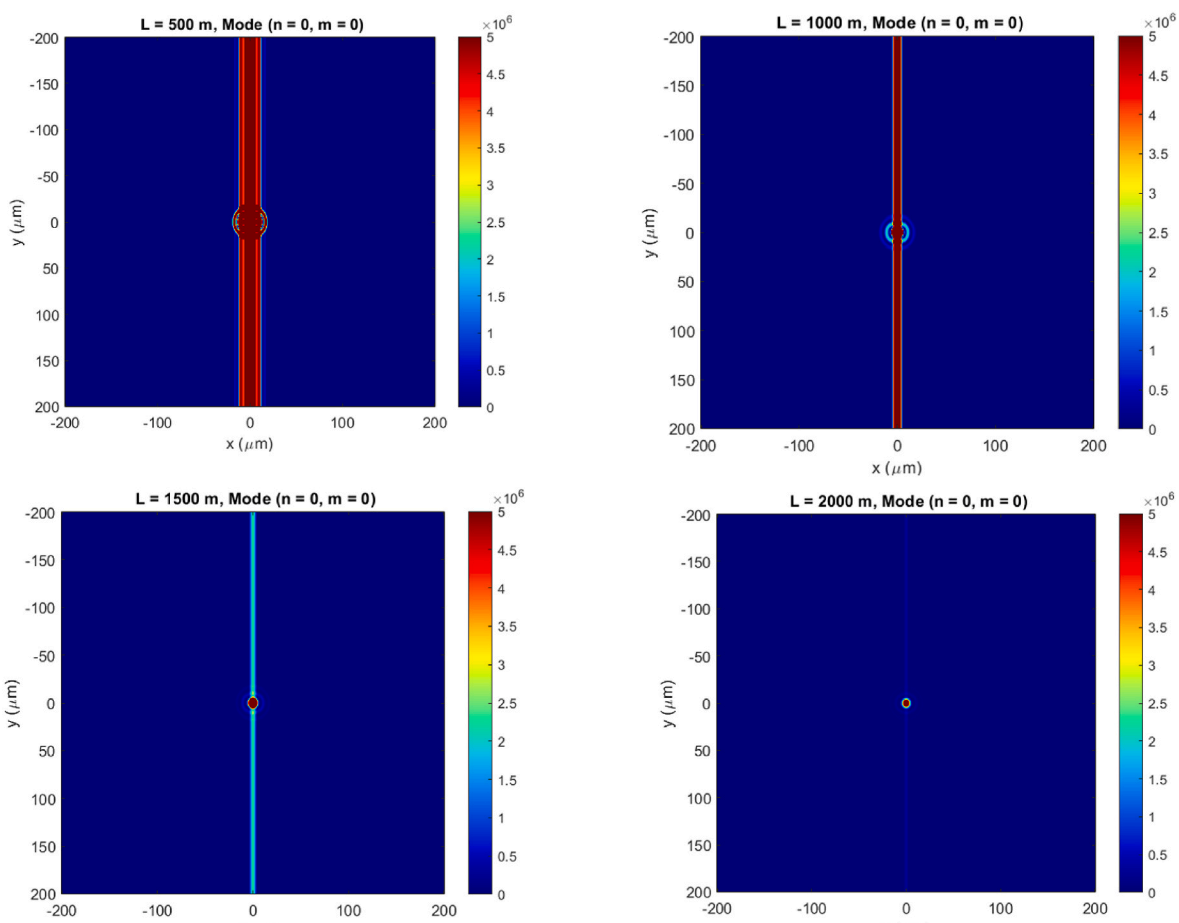

Fig. 4. Number of Photons at focal plane for m = 0, n = 0 (Gaussian beam).

multiplied by the exposure time, taking into account the sensitivity of the camera. Additionally, the sensor's quantum efficiency, which denotes the effectiveness of converting photons into electrical signals, is considered in the calculation. When photons are absorbed by a CCD pixel, they generate electron-hole pairs that are collected in the pixel's potential well. The number of electrons collected is directly proportional to the number of incident photons during the exposure period. However, once the pixel reaches its saturation capacity, any additional photons that strike the pixel cannot be collected, resulting in photon spillover into neighboring pixels.

The number of photons that can be converted into an electron by each pixel of CCD sensor can be defined by following equation:

$$N_{photons} = \frac{IA_{pixel}\eta\tau}{E}$$

Where I intensity in focal plane obtained by eq. (21), $A_{pixel} = 1\ \mu m^2$ pixel area, $\eta = 0.3$ quantum efficient, $\tau = 1\ \mu s$ exposure time and E energy of each photon.

Fig. 4 illustrates the number of converted photons by a CCD camera at the focal plane after the propagation of a Gaussian beam over distances of L = 500 m, 1000 m, 1500m, 2000 m. While the beam maintains a Gaussian intensity profile, the images clearly show saturation and blooming effects, primarily caused by exceeding the well capacity of the CCD pixels. This saturation leads to leakage of charge into neighboring pixels, resulting in the characteristic blooming halo. Additionally, inherent leakage in CCD pixels contributes to charge diffusion, further impacting the accuracy of the recorded photon distribution. At L = 500 m, the photon density at the focal plane is highly concentrated, causing significant saturation at the beam center and prominent blooming, particularly in the vertical direction. This vertical elongation reflects both photon leakage due to well saturation and the inherent charge diffusion within the pixel structure. As the propagation distance increases to L = 1000 m, and 1500 m, the beam spreads, reducing the central intensity and alleviating saturation. However, some blooming remains due to both residual photon concentration and inherent leakage effects. At L = 2000 m, the beam is significantly broadened, resulting in a more even photon distribution and minimal saturation or blooming.

The inherent leakage in CCD pixels (Ruyten, 1999), a result of charge diffusion, plays a secondary but notable role in these observations. Even without saturation, charge can diffuse from one pixel to adjacent pixels, blurring the recorded intensity distribution. This inherent characteristic of CCD sensors, coupled with blooming from well saturation, underscores the challenges in accurately capturing high-intensity photon distributions. Mitigating these effects may involve using CCDs with higher well capacities, advanced pixel designs that limit leakage, or employing post-processing algorithms to correct for diffusion and blooming artifacts. These steps are crucial for applications requiring precise beam profiling and photon measurements, particularly in optical diagnostics and imaging systems.

Fig. 5 presents the number of photons converted to signal for a Laguerre-Gaussian beam in mode n = 2, m = 1 after propagation distances of L = 1000 m,400 m,350 m, and 300 m. The plots clearly show how the beam's spatial profile and photon absorption characteristics evolve with decreasing propagation distance, along with the effects of saturation and blooming. At L = 1000, the beam profile maintains a relatively well-defined, circular structure typical of the Laguerre-Gaussian mode, with no observable saturation or blooming. The

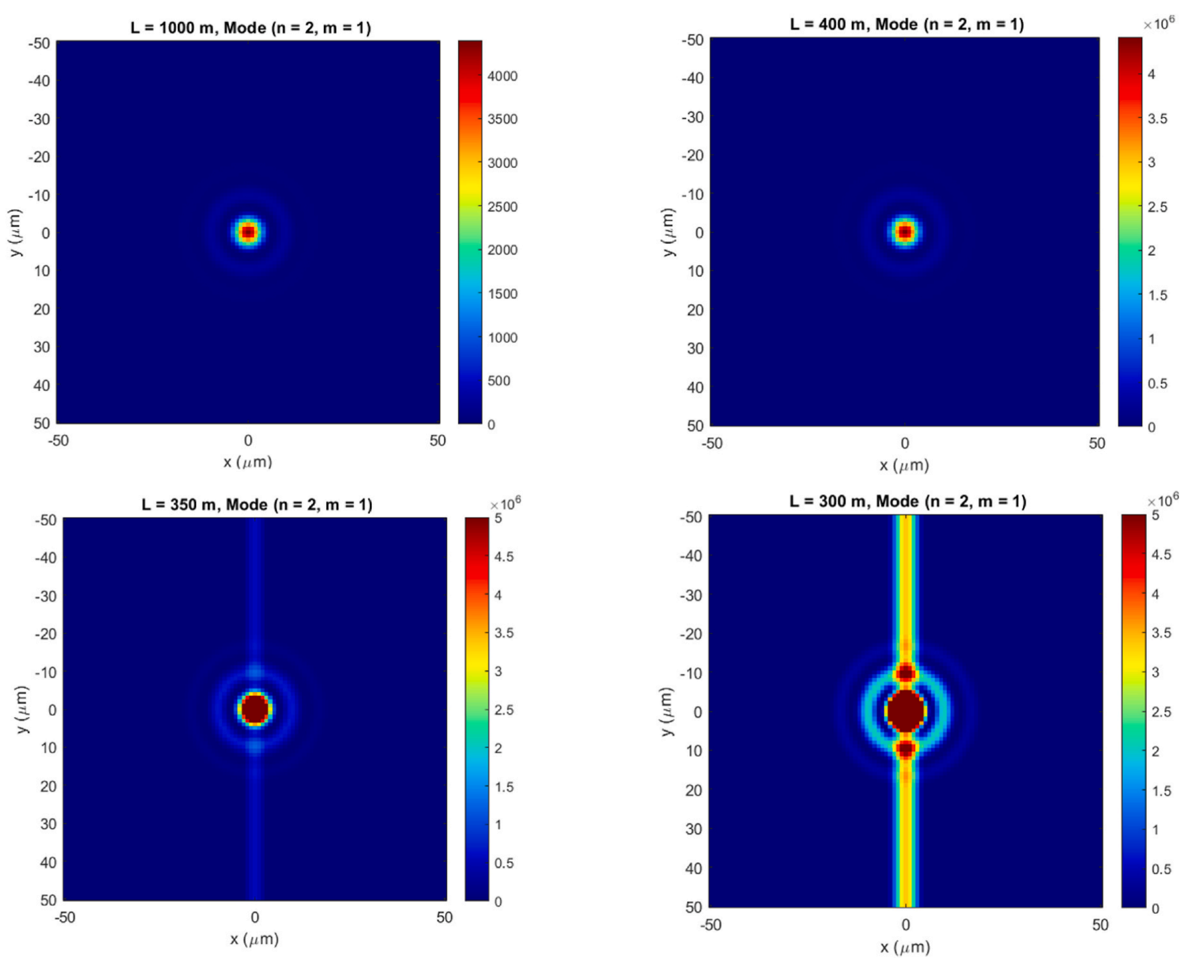

Fig. 5. Number of Photons at focal plane for m = 2, n = 1 (Laguerre-Gaussian beam).

photon counts are lower, and the intensity distribution is more uniform. As the propagation distance decreases to L = 400 m, the central intensity increases, but the beam still retains its characteristic shape with no significant artifacts. At shorter distances, the photon density increases sharply, leading to saturation at the central peak. This is evidenced by the bright red core in the intensity map. Saturation results in blooming, visible as vertical streaks in the plots caused by charge leakage from the saturated pixels.

These observations emphasize the trade-off between beam propagation distance and CCD sensor performance in capturing high-intensity photon distributions. While longer distances reduce saturation and blooming, shorter distances result in higher photon densities that challenge the dynamic range and capacity of the CCD. The artifacts seen here, such as saturation and vertical blooming, underscore the importance of selecting suitable sensor technologies or employing post-processing techniques to correct for these effects. Additionally, the Laguerre-Gaussian beam's unique spatial structure requires careful analysis to ensure accurate profiling and minimize distortions caused by the sensor's limitations. These findings are critical for applications involving high-intensity beams, such as optical communication, beam shaping, or advanced imaging systems.

Fig. 6 demonstrates the effect of varying the f-number on the number of photons absorbed by a CCD camera at the focal plane for a fixed mode ($n = 3, m = 2$) and propagation distance. At lower f-numbers ($f = 1$) and ($f = 2$), the larger aperture results in a highly concentrated beam at the focal plane, leading to extreme saturation in the central region. This saturation causes significant blooming, evident in the vertical streaks due to charge leakage from the saturated pixels into adjacent ones along the vertical axis, a limitation of the CCD sensor. As the f-number increases ($f = 5$), the aperture size decreases, spreading the beam more evenly and significantly reducing the central saturation and blooming effects. Finally, at the highest f-number (($f = 10$), the narrow aperture spreads the beam over a larger area, eliminating saturation and blooming entirely, resulting in a smooth intensity profile. However, the central intensity decreases as the beam is spread more widely, trading off focus for reduced artifacts. This analysis highlights how f-number adjustments impact the balance between high photon density and minimizing saturation and blooming, with lower f-numbers suitable for high-intensity applications requiring advanced sensors or corrections, and higher f-numbers better for accurate, artifact-free beam profiling.

4. Conclusion

This study explores the propagation of laser beams with Gaussian and Laguerre-Gaussian profiles through atmospheric turbulence, analyzing their detection by charge-coupled device (CCD) sensors. By employing numerical simulations based on the Kolmogorov turbulence model, we quantified the effects of turbulence strength and propagation distance on beam intensity distribution and photon detection. The results demonstrate that atmospheric turbulence significantly impacts laser beam profiles, with higher turbulence levels causing substantial beam broadening and energy dispersion. For Gaussian beams, the Full Width at Half Maximum (FWHM) increased from 50 μm to 1.5 m under strong turbulence conditions ($Cn^2 = 10^{-12}$). Higher-order Laguerre-

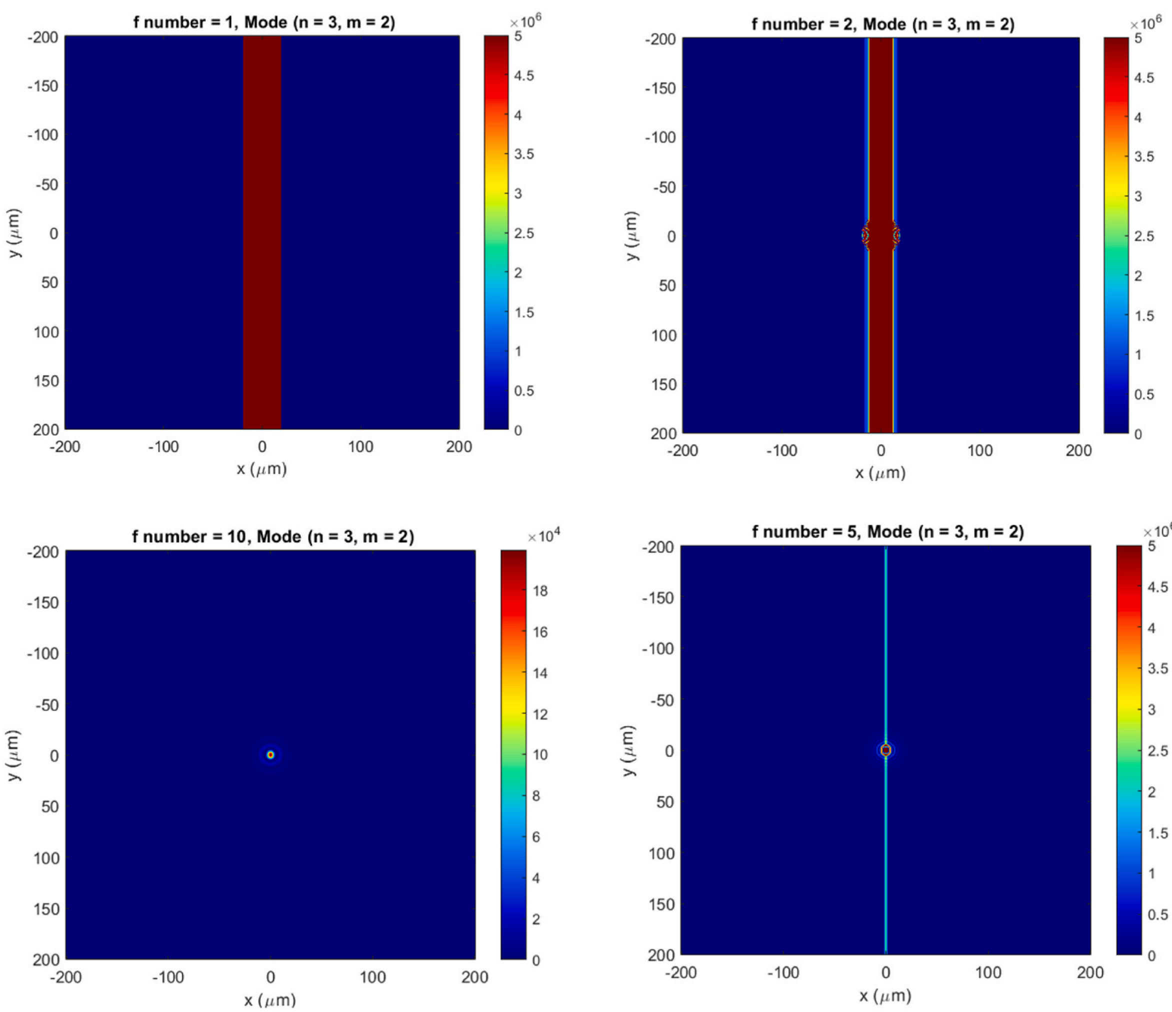

Fig. 6. Photon distribution at the focal plane for mode (n = 3, m = 2) with varying f-numbers.

Gaussian modes exhibited up to 90 % greater broadening compared to Gaussian modes, highlighting their sensitivity to turbulence. These findings underscore the trade-off between mode complexity and stability in turbulent environments.

At the CCD sensor, the study revealed saturation and blooming artifacts, particularly in high-intensity regions where photon densities exceeded 10^6 photons/pixel. These artifacts are attributed to the limited well capacity and inherent charge diffusion in CCD pixels. By adjusting aperture size and f-number, we demonstrated that increasing the f-number from 2 to 8 effectively reduced saturation by 60 %, spreading the beam over a larger area and mitigating artifacts.

CRediT authorship contribution statement

Maryam Jafari: Writing – original draft, Validation, Investigation. **Masoud Mollaee:** Writing – review & editing, Writing – original draft, Supervision. **Khashayar Heshmati Jannat Magham:** Writing – original draft, Data curation. **Mahmoud Rezaee Rokanabadi:** Supervision.

Availability of data and materials

All data generated or analyzed during this study will be made available upon request.

Declaration of competing interest

The authors declare that they have no known competing financial interests or personal relationships that could have appeared to influence the work reported in this paper.

Acknowledgement

This research was supported by Ferdowsi University of Mashhad.

Data availability

Data will be made available on request.

References

Andrews, L.C., Phillips, R.L., 2005. Laser Beam Propagation Through Random Media. SPIE Press.

Andrews, L.C., Al-Habash, M.A., Hopen, C.Y., Phillips, R.L., 2001. Theory of optical scintillation: gaussian-Beam wave model. WRM 11 (3), 271–291. https://doi.org/10.1080/13616670109409785.

Ata, Y., 2022. Structure function, coherence length, and angle-of-arrival variance for gaussian beam propagation in turbulent waters. JOSA A 39 (1), 63–71. https://doi.org/10.1364/JOSAA.444304. Vol. 39, Issue 1, pp. 63–71.

Dickson, L.D., 1970. Characteristics of a propagating Gaussian beam. Appl. Opt. 9 (8), 1854. https://doi.org/10.1364/ao.9.001854.

Hashemipour, S.H., SalmanOgli, A., Mohammadian, N., 2012. The effect of atmosphere disturbances on laser beam propagation. Key Eng. Mater. 500, 3–8. https://doi.org/10.4028/WWW.SCIENTIFIC.NET/KEM.500.3.

Huang, Y., Gao, Z., Zeng, A., Zhang, B., 2015. Beam wander of partially coherent array beams through Non-Kolmogorov turbulence. Opt. Lett. 40 (8), 1619–1622. https://doi.org/10.1364/OL.40.001619. Vol. 40, Issue 8, pp. 1619–1622.

Korotkova, O., Andrews, L.C., Phillips, R.L., 2004. Model for a partially coherent gaussian beam in atmospheric turbulence with application in lasercom, 43 (2), 330–341. https://doi.org/10.1117/1.1636185.

Luo, C., Han, X., 2020. Evolution and beam spreading of arbitrary order vortex beam propagating in atmospheric turbulence. Opt. Commun. 460, 124888. https://doi.org/10.1016/J.OPTCOM.2019.124888.

Ronchi, L., Consortini, A., Stefanutti, L., 1970. Investigation of atmospheric turbulence by narrow laser beams. Appl. Opt. 9 (11), 2543–2547. https://doi.org/10.1364/AO.9.002543. Vol. 9, Issue 11, pp. 2543–2547.

Ruyten, W., 1999. Smear correction for frame transfer charge-coupled-device cameras. Opt. Lett. 24 (13), 878–880. https://doi.org/10.1364/OL.24.000878 vol. 24, no. 13, pp. 878–880.

Salem, M., Korotkova, O., Dogariu, A., Wolf, E., 2004. Polarization changes in partially coherent electromagnetic beams propagating through turbulent atmosphere. Waves Random Media 14 (4), 513–523. https://doi.org/10.1088/0959-7174/14/4/003.

Sayan, Ö.F., Gerçekcioğlu, H., Baykal, Y., 2020. Hermite gaussian beam scintillations in weak atmospheric turbulence for aerial vehicle laser communications. Opt. Commun. 458, 124735. https://doi.org/10.1016/J.OPTCOM.2019.124735.

Shaik, K.S., 1988. Atmospheric propagation effects relevant to optical communications. TDA Prog. Rep.

Yahel, R.Z., Last, I., 1992. Numerical simulation of laser beam propagation in three-dimensional random media: beam splitting and patch formation. Waves Random Media 2 (1), 81. https://doi.org/10.1088/0959-7174/2/1/007.